CHEM.4008/4061.
2004/2005.
Electroactive Nanostructured Materials.

Dr Mike Lyons
Chemistry Department
Room 2.02 SNIAM.
Email: melyons@tcd.ie

Electroactive Nanostructured Materials.

Lecture 1/2.

Course Summary.

- 4/6 lectures. 4 lectures for SS Chemists, 6 lectures for SS Advanced Materials. These will will mainly cover:
  - Introduction to electroactive nanostructured materials.
  - Self assembled electroactive monolayers and monolayer protected clusters (MPC's).
  - Electronically conducting polymer materials.
  - Redox polymer materials.
  - Catalysis/sensing using electroactive polymer thin films.
  - Transport and kinetics within electroactive polymer thin films : theory and experiment.
- Main reference : Electroactive polymer electrochemistry (Lyons), Plenum Press, 1994/1996, available in Hamilton Library. Also some review articles which will be given out during course.

Electroactive Nanostructured Materials

Motivations/Introduction.

Electroactive nanostructured materials.

- Electroactive materials can be assembled on the surface of a support electrode to form a 'tailormade' or chemically modified electrode (CME).
- The electrode surface may be modified either with an ordered monolayer film or a multilayer polymer film.
- These materials exhibit a capacity to:
  - Pass electric current.
  - Store charge.
  - Display redox activity.
    - Sites in monolayer/polymer film may undergo oxidation/reduction when a potential is applied to the material.
- Applications:
  - Battery materials
  - Electrochromic displays
  - Microelectronic devices
  - Molecular electronics
  - Electrocatalysis
  - Chemical/biological sensor technology
  - Energy conversion
  - Corrosion protection
  - Actuators.

Chemically Modified Electrodes.

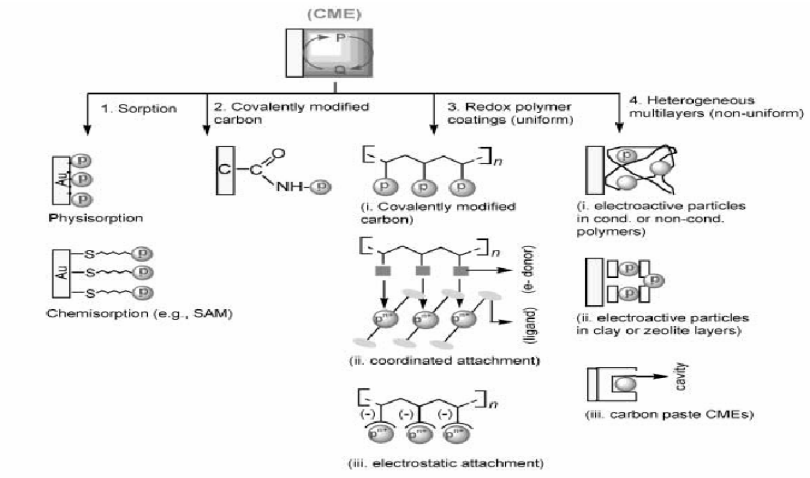

Nanoscience and Nanotechnology.

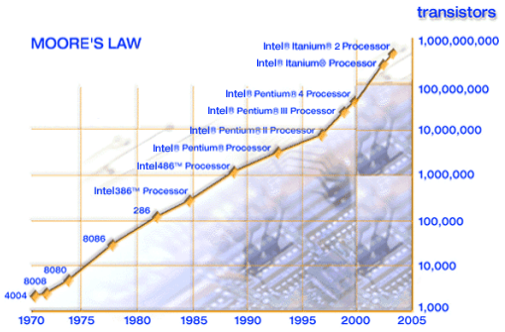

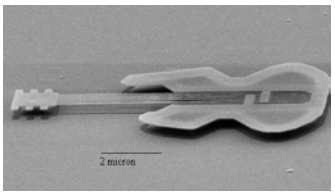

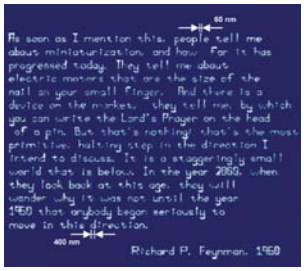

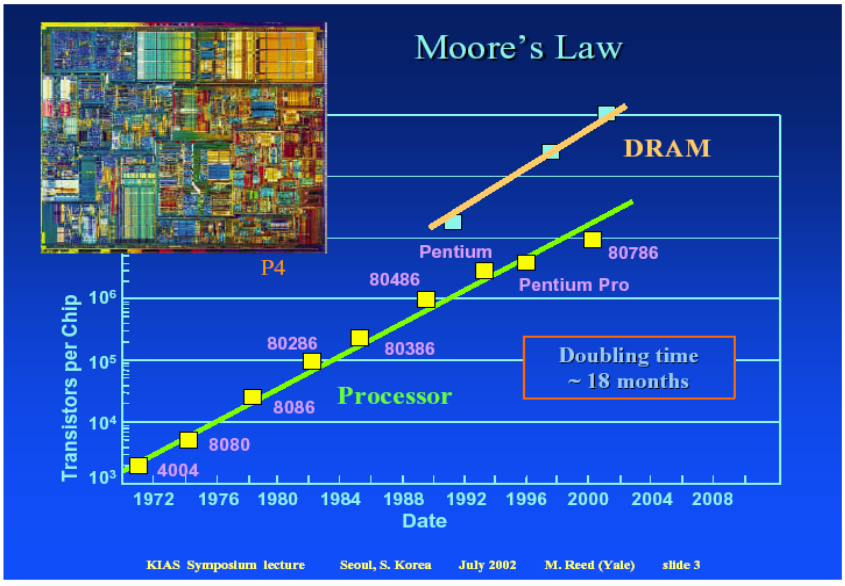

Small is beautiful !
Molecular Electronics.

The Molecule–Electrode Interface in Single-Molecule Transistors**

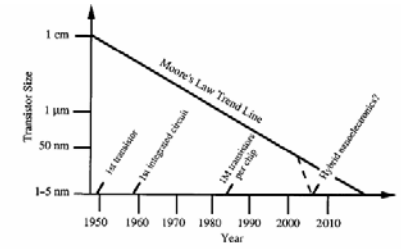

Fig. 1 "Moore's Law" plot of transistor size vs. year. The trend line illustrates the fact that the transistor size has decreased by a factor of 2 every 18 months since 1950.

*Hongbin Yu, Yi Luo, Kristen Beverly, J. Fraser Stoddart, Hsian-Rong Tseng, and James R. Heath**

Angew. Chem. Int. Ed. **2003**, *42*, 5706–5711

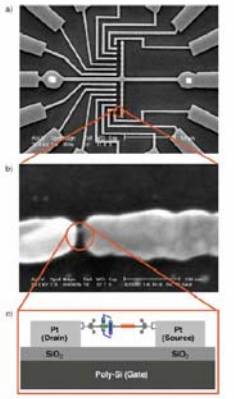

Figure 1. a) Scanning electron microscope (SEM) pictures of single-molecule devices fabricated on a Si substrate. A 30-nm thick low-temperature thermal oxide of Si was grown on top of a degenerately doped Si substrate. The center metal electrode, where the break junction is made of 7-nm thick Pt, followed by 100-nm thick gold wires and pads for wire bonding. b) The SEM image after the break junction is made. The separation between the two metal electrodes is around 4 nm. c) A section through a single-molecule transistor.

Molecular Electronics/ICT

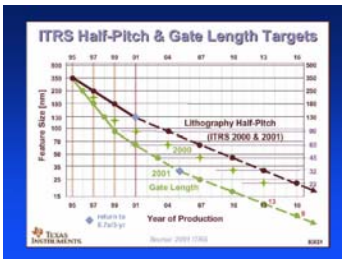

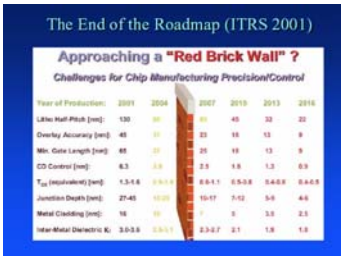

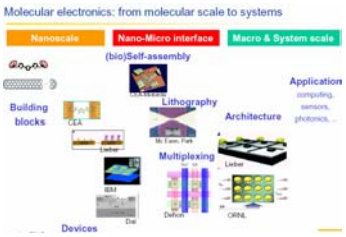

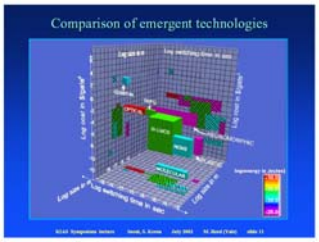

Electronic conduction in nanodevices

- **The Good:** principles of electron transport in the solid state are essentially understood, because the contact technology exists
- **The Bad:** contacts have always been the problem with every new device technology, and it has always been solved by alchemy
- **The Ugly:** in true atomic/molecular systems, the device & the contact is no longer separable (mesoscopics conveniently sidesteps this due to length scales; i.e., the device is mostly depletion layer)

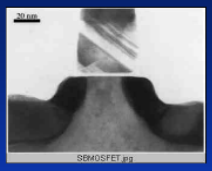

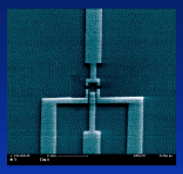

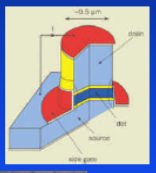

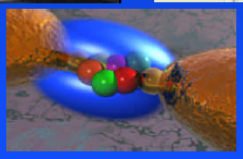

Single Molecule Measurements

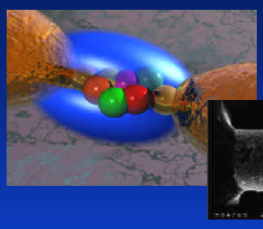

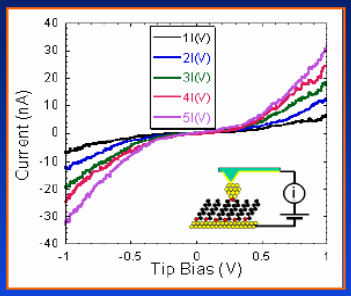

Cui *et. al*, Science 294, 571 (2001)

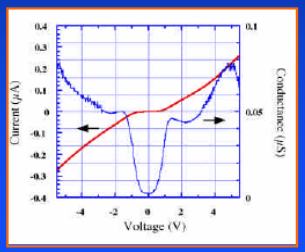

Reed *et. al*, Science 278, 252 (1997)

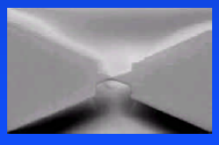

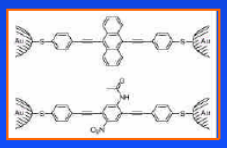

Reichert *et. al*, PRL 88, 176804 (2002)

Chemical/Biological Sensor Configuration.

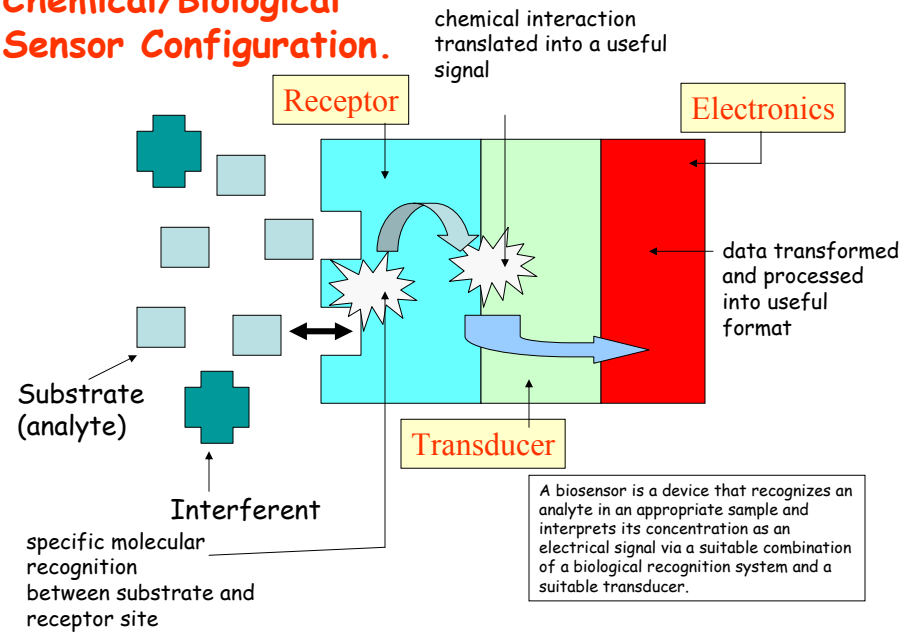

Mediated Electron Transfer

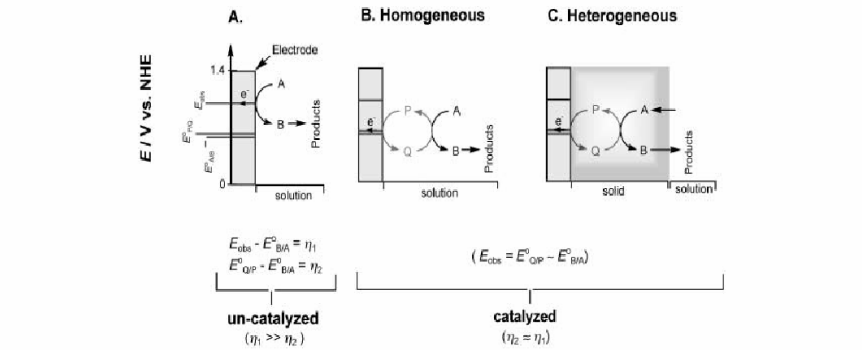

Fig. 1. Schematic representation for the oxidation reaction of A → B on bare (A) and mediated conditions (B, C). The terms P and Q correspond to the reversible mediator of reduced and oxidized states, respectively. The E_{obs}, $E^{0}_{P/Q}$, $E^{0}_{A/B}$ and η correspond to uncatalyzed, P/Q mediated, standard and over potentials, respectively, for the above mentioned reaction. In homogenous catalyzed reaction, the P/Q mediator and reactant are in solution phase; while for heterogeneous catalyzed reaction, the P/Q is bonded on the electrode surface.

Enzyme communication with electrodes.

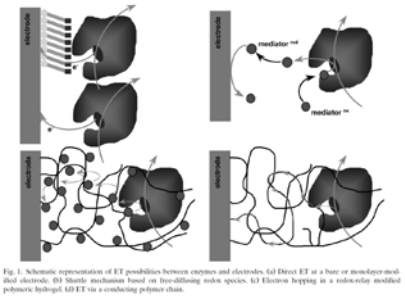

W. Schuhmann / Reviews in Molecular Biotechnology 82 (2002) 425–441

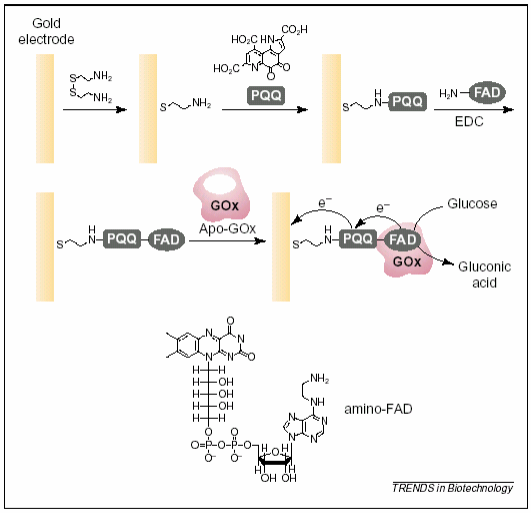

Fig. 2. The surface-reconstitution of apo-glucose oxidase on a PQQ-FAD monolayer assembled on a gold electrode. Abbreviations: EDC, 1-ethyl-3-(3-dimethylaminopropyl)-carbodiimide; FAD, flavinadenine dinucleotide; GOx, glucose oxidase; PQQ, pyrrolquinoline quinone.

Amperometric enzyme biosensor for glucose measurement.

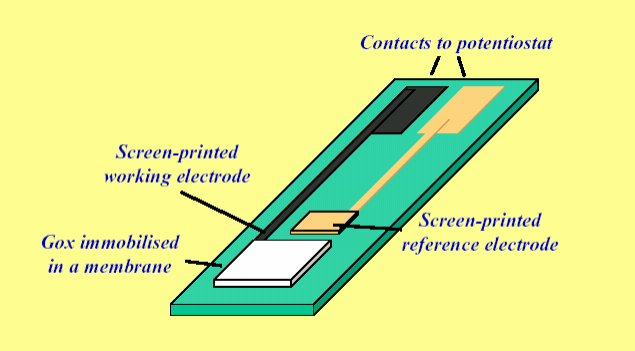

Enzyme biosensor: uses electron transfer mediator in electrochemical detection step.

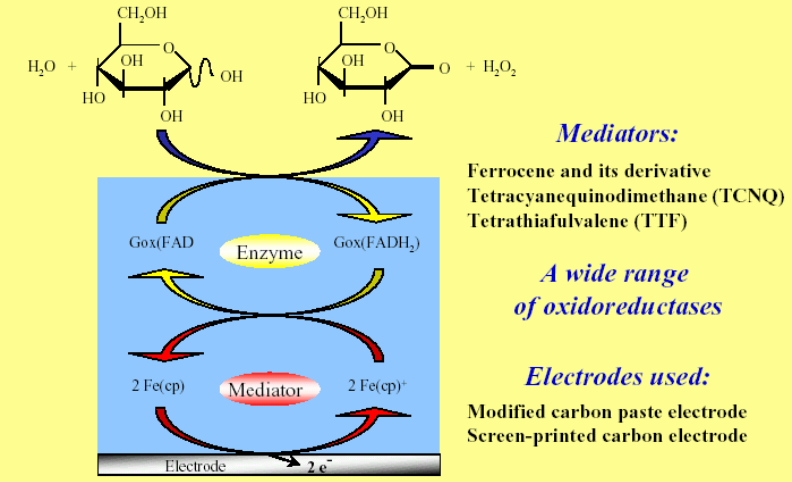

Mediators:

Ferrocene and its derivative
Tetracyanequinodimethane (TCNQ)
Tetrathiafulvalene (TTF)

A wide range of oxidoreductases

Electrodes used:

Modified carbon paste electrode
Screen-printed carbon electrode

Self Assembled Monolayers (SAM)

Fundamental Properties.

Chemically modified electrodes: 2D vs 3D nanostructures.

- Monolayer derivitized electrodes developed first.
- New interest in these systems:
  - Redox active self assembled monolayers. e.g. ferrocene containing alkane thiols.
- CME systems based on 3D microstructures. E.g. electroactive polymer thin films such as poly(vinylferrocene), poly(pyrrole).
- These materials are preferable for chemical sensor and electrocatalytic systems, since there is a 3D dispersion of active sites throughout the material and a high concentration of active sites is achieved even though the quantity of active material is small.

Monolayer vs multilayer modified electrodes.

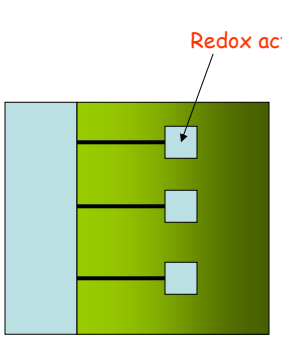

2D nanostructure.
Redox active monolayer.
Surface coverage ca. 10^{-10} mol cm^{-2}.

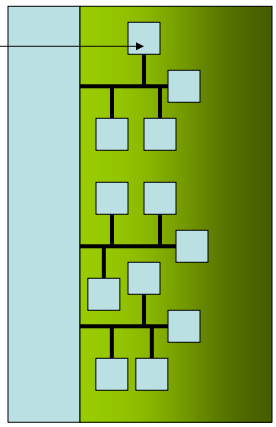

3D nanostructure.
Redox active multilayer.
Surface coverage ca. 10^{-8} molcm^{-2}

Alkanethiol SAM's: Ordered nano-assemblies.

- The formation of organized monolayers at metallic surfaces through self assembly provides an attractive method for the preparation of nanostructured ensembles with well defined composition, structure and thickness.
- These **self assembled monolayers** (SAM) have been used as model systems to test modern theories of interfacial electron transfer dynamics across organic spacers in a controlled manner.
- Redox active SAM ensembles, consisting of ferrocene units covalently attached to alkane thiol connectors adsorbed on gold substrate surfaces, especially when mixed and diluted with non-electroactive alkane thiols, also serve as good mechanically robust models for molecular wires and individual molecular nanoelectrode systems.

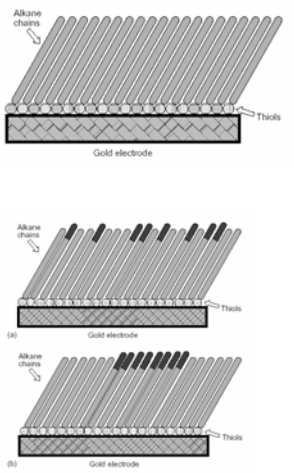

n-alkyl Self Assembled Systems

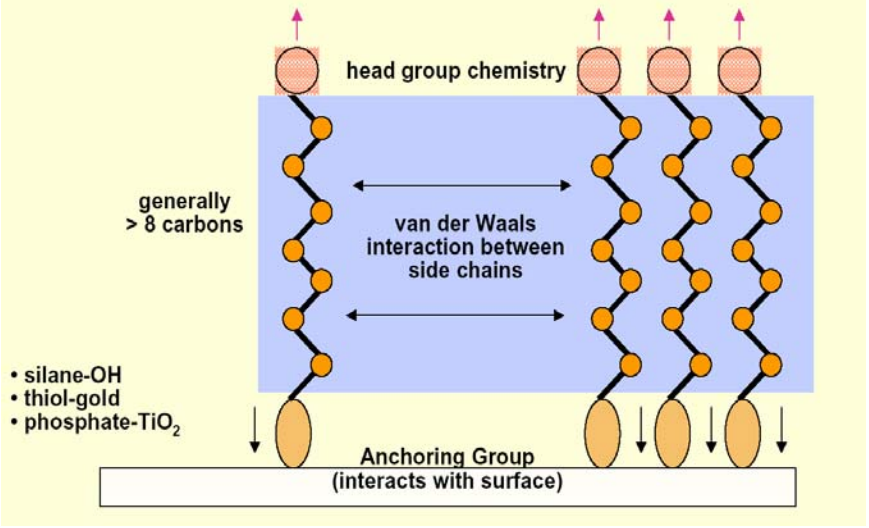

n-Alkyl Thio Self-Assembly on Gold (111)

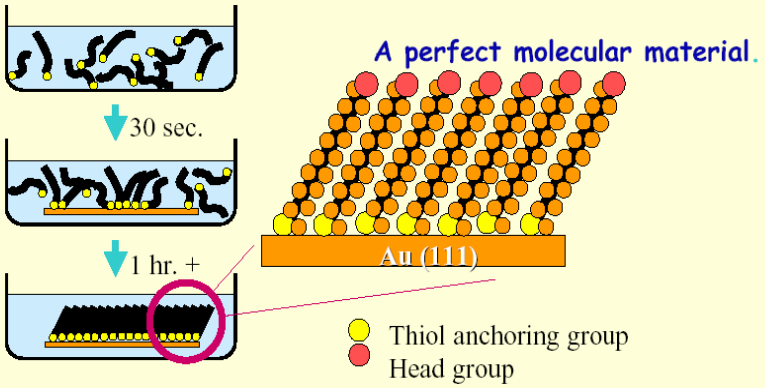

Major discovery -- 1983

Nuzzo,RG; Allara,DL (1983): Adsorption of bifunctional organic disulfides on gold surfaces. J. Am. Chem. Soc. 105(13), 4481-4483.

Alkane thiol SAM formation.

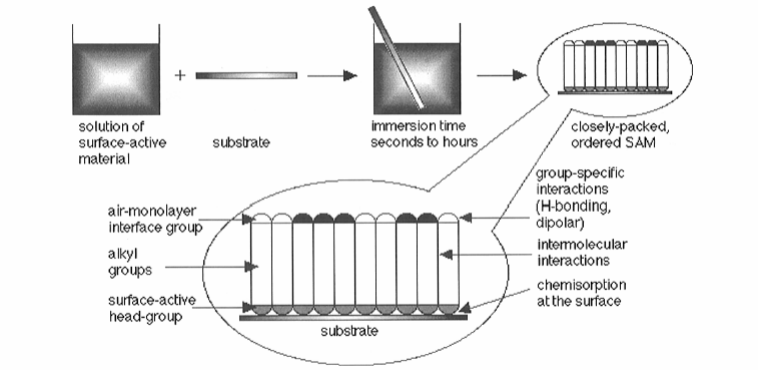

Oxidative addition of SH bond to Au surface followed by reductive elimination of hydrogen.

$$R{-}S{-}H + Au_n^0 \rightarrow R{-}S^-Au^+ \cdot Au_n^0 + {}^1/_2H_2$$

Alkanethiol SAM Formation

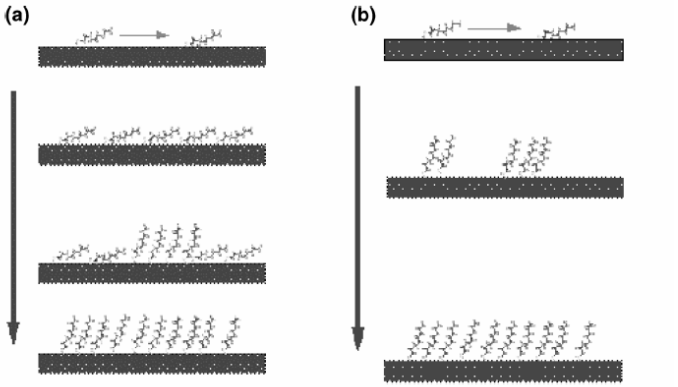

Fig. 6.5. Schematic drawing of the initial stage of alkanethiol SAM growth: (**a**) in vacuum or low-concentration solution; (**b**) in a higher-concentration solution

Alkanethiol Self Assembly Mechanism

Scheme I. Proposed reaction pathway

$$C_{18}SH\ [\text{solution,C}] + Au(111)\ [\text{empty sites}] \underset{k_{-1}}{\overset{k_1}{\rightleftarrows}} C_{18}SH/Au(111)\ [\text{lying-down}],$$

$$C_{18}SH/Au(111)\ [\text{lying-down}] + C_{18}SH/Au(111)\ [\text{lying-down}] \xrightarrow{k_2} 2C_{18}S/Au(111)\ [\text{standing-up}],$$

$$C_{18}SH/Au(111)\ [\text{lying-down}] \xrightarrow{k_2'} C_{18}S/Au(111)\ [\text{standing-up}].$$

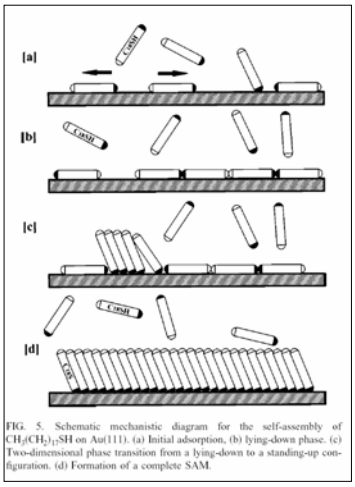

FIG. 5. Schematic mechanistic diagram for the self-assembly of $CH_3(CH_2)_{17}SH$ on Au(111). (a) Initial adsorption, (b) lying-down phase. (c) Two-dimensional phase transition from a lying-down to a standing-up configuration. (d) Formation of a complete SAM.

SAM Formation : Adsorption kinetics.

Adsorption usually occurs on a far shorter timescale (minutes) than self Assembly (hours, days).
We model the adsorption process via a Langmuir Isotherm.
Controversy exists regarding the exact nature (electrochemical vs non-electrochemical) of the adsorption mechanism.

$$M + RS - H \rightarrow RS - M + \frac{1}{2}H_2$$

Traditional non EC mechanism

$$RS - H + M \rightarrow RS - M + H^+ + e^-$$

New EC mechanism

Adsorption process examined usually via optical (Second Harmonic Generation SHG) or gravimetric (electrochemical quartz crystal microbalance EQCM) techniques.
Adsorption occurs mainly by dipping metal support into solution containing alkane thiol at low concentration (0.1 μM-1 mM) either at open circuit but also when the metal is subjected to an applied potential (typically 0.2-0.6 V).
Monolayer film formed under potential control exhibits better packing and order and forms much more rapidly.

EQCM Fundamentals.

- The quartz crystal microbalance (QCM) is a variant of acoustic wave microsenseors that are capable of ultrasensitive mass measurements. Under favorable conditions, a typical QCM can measure a mass change of 0.1-1 ng/cm^2.
- The QCM oscillates in a mechanically resonant shear mode (determined by the dimensions of the crystal and the mass loading) under the influence of a high frequency AC electric field which is applied across the thickness of the crystal. A change in the mass of the working electrode causes a change in the resonant frequency of the piezoelectric device, which can then be related directly to the quantity of added mass via the Sauerbrey equation:

$$\Delta f = -C_f \Delta m \qquad C_f = \frac{2 f_0^2}{\sqrt{\rho \mu A}}$$

  where C_f is a constant which depends on the density ρ of the crystal, μ the shear modulus of quartz , the area A of the gold coated quartz disc , and f_0 the resonant frequency of the fundamental mode of the crystal.
- Hence an increase in mass implies a decrease in frequency and one can use small changes in frequency to monitor very small changes in mass in a very accurate manner.

Electrochemical Quartz Crystal Microbalance.

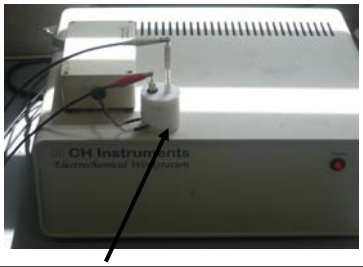

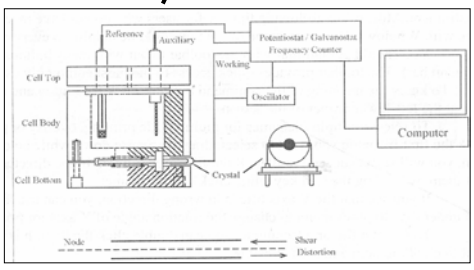

Sauerbrey Equation

$\triangle f = [-2f_0^2 / A(\mu\rho)^{1/2}] \triangle m$

For:

$\triangle f = 1Hz$

$\Rightarrow \triangle m = 1.4ng$

$$\Delta f = -C_f \Delta m = -\frac{M}{nF} \Delta Q$$

$$C_f = \frac{2}{\sqrt{\rho \mu}} f_0^2$$

$\Delta f \downarrow as\ \Delta m \uparrow$

EQCM: thiol adsorption

Lee et al.
Bull. Kor. Chem. Soc. 2001,22,276

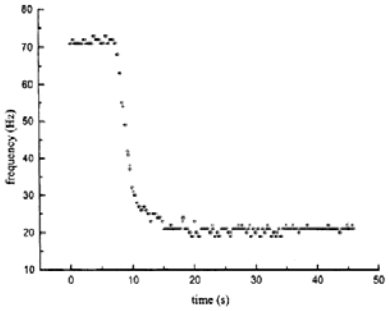

Figure 1. Representative raw data of QCM oscillation frequency vs time subsequent to thiol injection. Injected solution was $C_{18}H_{37}SH$/*n*-hexane. See text for a detailed discussion of these data.

Karpovich and Blanchard

Langmuir **1994,** *10,* 3315−3322

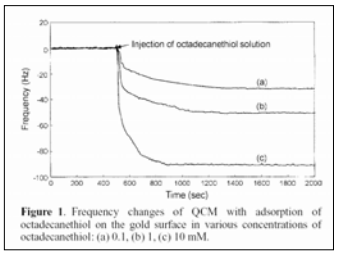

Figure 1. Frequency changes of QCM with adsorption of octadecanethiol on the gold surface in various concentrations of octadecanethiol: (a) 0.1, (b) 1, (c) 10 mM.

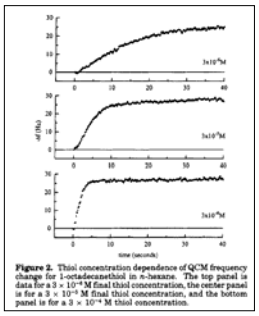

Figure 2. Thiol concentration dependence of QCM frequency change for 1-octadecanethiol in *n*-hexane. The top panel is data for a 3×10^{-4} M final thiol concentration, the center panel is for a 3×10^{-5} M final thiol concentration, and the bottom panel is for a 3×10^{-6} M thiol concentration.

Langmuir Adsorption Isotherm

SAM coverage expressed in terms of the fractional surface coverage θ with 0≤θ≤1. The latter quantity represents the fraction of available sites which have reacted.

$$\theta = \frac{\Gamma}{\Gamma_m} = \frac{N_U}{N_\Sigma}$$

Total # sites: $N_\Sigma = N_U + N_V$ (# vacant sites + # occupied sites)

Net rate of adsorption

$$\frac{d\theta}{dt} = k_A(1-\theta)c - k_D\theta$$

Adsorption rate Constant $M^{-1}s^{-1}$; Desorption rate Constant s^{-1}

Γ= surface coverage (typically nmol/cm² range)
Γ_m = monolayer surface coverage

Integrate rate eqn. using initial condition : θ = 0, t = 0

$$\kappa = \frac{c}{c + \frac{k_D}{k_A}}$$

Adsorbate concentration

$$\theta(t) = \frac{c}{c + k_D/k_A}\left\{1 - \exp\left[-(k_A c + k_D)t\right]\right\}$$

$$\theta(t) = \kappa\left(1 - \exp\left[-k_{obs}t\right]\right)$$

$$k_{obs} = k_A c + k_D$$

Diagnostic Plot

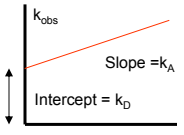

Equilibrium constant K (M^{-1})

$$K = \frac{k_A}{k_D}$$

Gibbs energy of adsorption

$$\Delta G_{ads} = -RT \ln K$$

Steady state fractional coverage $\theta(\infty)$ occurs when t → ∞

$$\theta(\infty) = \frac{Kc}{1 + Kc}$$

Table 3. Fractional Surface Coverage as a Function of Thiol Concentration, Calculated Using Equation 6, for the 1-Octadecanethiol/*n*-Hexane System[a]

thiol concentration (M)	$\theta(\infty)$
3×10^{-6}	0.04 ± 0.02
1×10^{-5}	0.13 ± 0.07
3×10^{-5}	0.31 ± 0.16
1×10^{-4}	0.60 ± 0.34
3×10^{-4}	0.82 ± 0.51

[a] The uncertainty in $\theta(\infty)$ is determined by propogation of the uncertainty in k_a and k_d.

Table 4. K_{eq} and ΔG_{ads} Determined from the Experimental Data[a]

adsorbate/solvent	K_{eq} (M^{-1})	ΔG_{ads} (kcal/mol)
1-octadecanethiol/*n*-hexane	15250 ± 7300	−5.6 ± 0.2
1-octadecanethiol/cyclohexane	10850 ± 8950	−5.5 ± 0.4
1-octanethiol/*n*-hexane	1930 ± 840	−4.4 ± 0.2

[a] Uncertainty in ΔG_{ads} is propogated from the uncertainty in K_{eq}.

Langmuir Model provides convenient first approach to extract quantitative kinetic and thermodynamic data for thiol adsorption from solution.

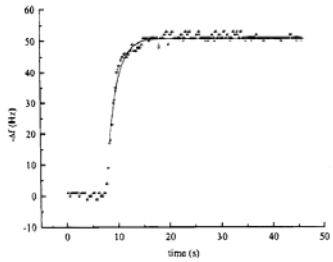

Figure 3. Fit of Langmuir adsorption isotherm (eq 4) to raw experimental data.

Table 1. k_{obs} Values Determined from Raw Data as a Function of Thiol Concentration

adsorbate/solvent	thiol concentration (M)	k_{obs} ± 95% C.I. (s^{-2})
1-octadecanethiol/ cyclohexane	1×10^{-5}	0.06 ± 0.02
	3×10^{-5}	0.23 ± 0.07
	1×10^{-4}	0.51 ± 0.16
	3×10^{-4}	0.58 ± 0.43
1-octadecanethiol/ *n*-hexane	1×10^{-6}	0.06 ± 0.04
	3×10^{-6}	0.14 ± 0.04
	1×10^{-5}	0.24 ± 0.06
	3×10^{-5}	0.23 ± 0.13
	1×10^{-4}	0.44 ± 0.16
	3×10^{-4}	0.75 ± 0.41
1-octanethiol/*n*-hexane	1×10^{-5}	0.17 ± 0.03
	3×10^{-5}	0.44 ± 0.06
	1×10^{-4}	0.52 ± 0.11
	3×10^{-4}	0.70 ± 0.23
	1×10^{-3}	1.20 ± 0.34
	3×10^{-3}	0.90 ± 0.34

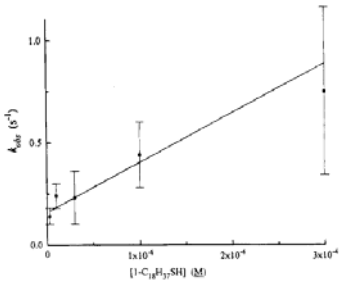

Figure 4. Concentration dependence of k_{obs} for 1-octadecanethiol in *n*-hexane in the concentration range over which Langmuir behavior is followed (see text for a discussion). The best fit line through the data has a slope of k_a and an intercept of k_d. See Table 2 for results of the fits to the data.

Table 2. k_a and k_d Determined from Concentration Dependence of k_{obsd}

adsorbate/solvent	k_a (M^{-1} s^{-1}) ± 95% C.I.	k_d (s^{-1}) ± 95% C.I.
1-octadecanethiol/cyclohexane	2059 ± 1394	0.19 ± 0.09
1-octadecanethiol/*n*-hexane	2440 ± 1074	0.16 ± 0.03
1-octanethiol/*n*-hexane	811 ± 334	0.42 ± 0.06

Self Assembly Kinetics

Optical monitoring of adsorption/ Self assmbly

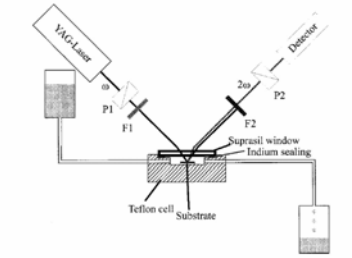

Figure 1. Scheme of the experimental setup of second harmonic generation at surfaces. P1 and P2 are polarizers, F1 and F2 are filters for blocking second harmonic and fundamental light, respectively. ω denotes the fundamental laser light at 1064 nm, 2ω the frequency-doubled light at 532 nm.

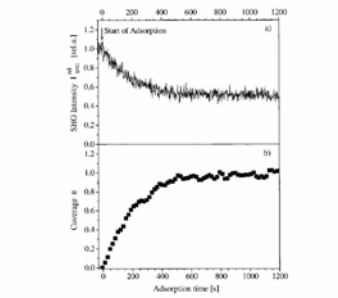

Figure 2. (a) Representative in situ SHG measurement of thiol adsorption. The example shows the adsorption of docosanethiol (C_{22}-SH) onto gold from 2.0 μM solution in ethanol. The fundamental wavelength is 1064 nm, the polarization is pp. (b) Time dependence of the coverage $\theta(t)$ (◆) calculated from (a) using eq 5. One data point represent the average of nine data points from (a).

O. Dannenberger,† M. Buck,* and M. Grunze

J. Phys. Chem. B **1999,** *103,* 2202−2213

Fit to Langmuir Adsorption Isotherm.

SAM surface structure

- STM & AFM very useful to obtain surface topography of alkanethiol SAMs.
- 2 types of coexisting molecular lattices observed for SAMs on Au(111) surfaces
  - (√3x√3)R30°structure
  - C(4x2) superstructure

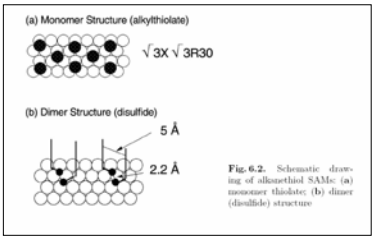

Fig. 6.2. Schematic drawing of alkanethiol SAMs: (a) monomer thiolate; (b) dimer (disulfide) structure

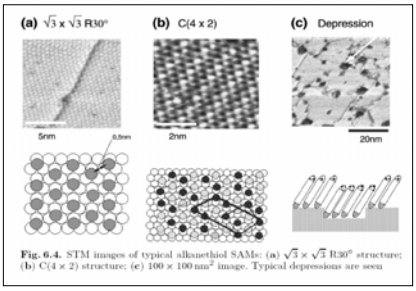

Fig. 6.4. STM images of typical alkanethiol SAMs: (a) $\sqrt{3} \times \sqrt{3}$ R30° structure; (b) C(4 × 2) structure; (c) 100 × 100 nm^2 image. Typical depressions are seen

$\sqrt{3}\times\sqrt{3}$ R30° C_6 lattice on Au(111)

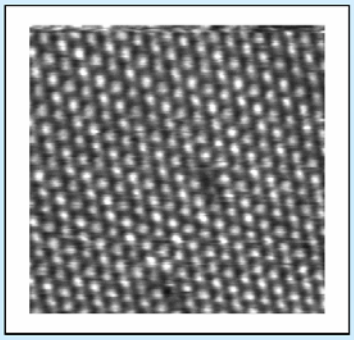

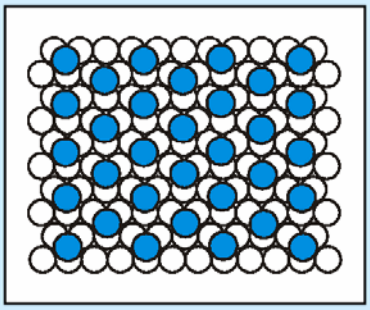

S-S distances are **0.5 nm**
7×7 nm^2 image

All sites are equivalent

C6 c(4×2) superlattices of the $\sqrt{3}\times\sqrt{3}$ R30°

(7.3×7.3 nm^2 images)

($2\sqrt{3} \times 3$)rect lattices

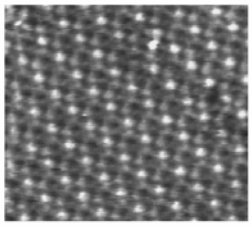

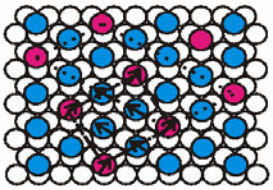

"Rectangular"
c(4 ×2)

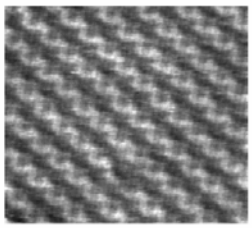

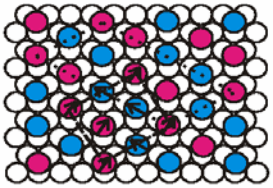

"Zig-zag"
c(4 ×2)

Modified Randles Equivalent Circuit Model : SAM coated metal

Alkane thiol film modelled as simple parallel plate capacitor.

$$\frac{1}{C_{DL}} = \frac{1}{C_{SAM}} + \frac{1}{C_D}$$
$$C_D >> C_{SAM}$$
$$C_{DL} \cong C_{SAM}$$

$$C_{SAM} = \frac{\varepsilon_0 \varepsilon_r}{L}$$

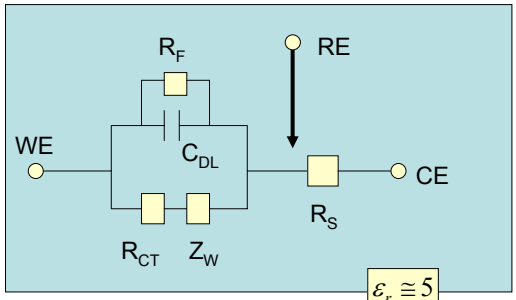

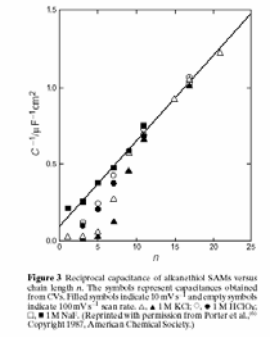

Figure 3 Reciprocal capacitance of alkanethiol SAMs versus chain length *n*. The symbols represent capacitances obtained from CVs. Filled symbols indicate 10 mV s^{-1} and empty symbols indicate 100 mV s^{-1} scan rate. △, ▲ 1 M KCl; ○, ● 1 M HClO$_4$; □, ■ 1 M NaF. (Reprinted with permission from Porter et al.,[86] Copyright 1987, American Chemical Society.)

Thiol film capacitance C_{SAM} inversely proportional to monolayer thickness L.

Layer thickness L proportional to thiol chain length n.

$\varepsilon_r \cong 5$

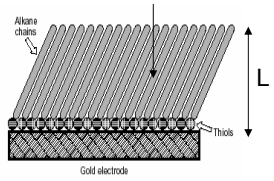

SAM Quality Control: Blocking solution phase interfacial ET reactions

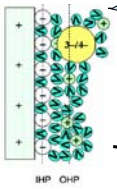

$Au / Fe(CN)_6^{4-/3-}(KCl(aq))$

$Au / SAM / Fe(CN)_6^{4-/3-}(KCl(aq))$

Poor monolayer: pinholes present.

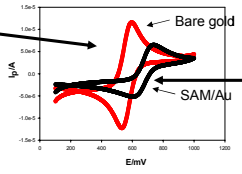

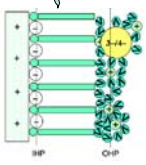

- Non redox active C12 alkanethiol monolayer generated via immersing gold substrate electrodes in 1mM dodecanethiol in EtOH solution for 48hrs.
- Integrity of monolayer formed via self assembly checked by immersion of electrode in 2mM Ferrocyanide/Ferricyanide solution in 1M KCl solution for 24 hrs and recording the resultant cyclic voltammogram.
- Ferrocyanide/ferricyanide redox behaviour well defined at bare gold electrode. In absence of pinholes in monolayer film no trace of ferrocyanide/ferricyanide redox activity should be observed since the ET kinetics of the solution phase redox couple will be effectively blocked because of greatly reduced electronic coupling between redox couple and Au electrode.

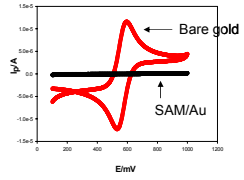

Good monolayer: redox activity of solution phase redox couple at underlying gold electrode blocked.

Redox active monolayers : alkanethiol self-assembled monolayers (SAM).

- Alkane thiol monolayer generated either via LB method or by self assembly.
- Both electroactive, non-electroactive, and'mixed' SAM systems readily generated.
- Wide range of redox groups can be attached to alkane chain : ferrocenes, quinones, azobenzenes, viologens, cytochrome c etc.
- Can readily achieve dilution of electroactive component in a mixed monolayer.
- Applications:
  - Microarray electrodes
  - Selective permeation
  - Pre-concentration & selective binding
  - Electrocatalysis
  - Long range ET
  - Corrosion and adhesion control.

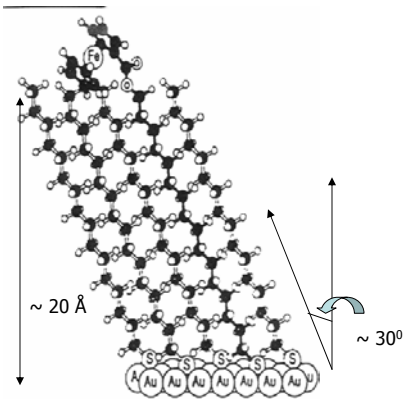

Co-adsorption of ferrocene-terminated alkane thiol and an unsubstituted alkane thiol on Au(111).

Redox labeled alkane thiols : Synthetic Strategy.

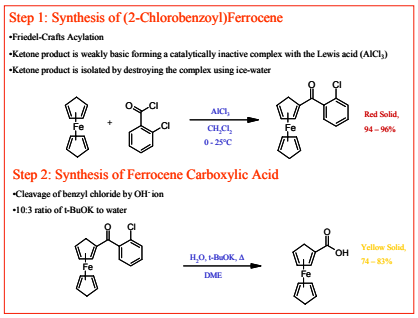

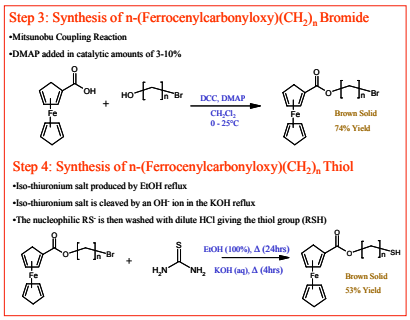

- Method suitable for preparation of C_5 – C_{12} alkane thiols.
- C_5 – C_{12} bromo-alcohols available commercially.

Redox switching in alkane thiol SAM's.

- Oxidative redox switching involves both a redox transformation Fc → Fc^+ (oxidation state change) and a coupled ion transfer/binding process to form ion pair Fc^+X^-. Reverse sequence occurs on reductive switching step.
- Can label reaction sequence as an EC process (E – redox ET, C – ion pair formation).
- ET chemistry and dynamics examined via cyclic voltammetry (CV).
- Ion pairing/transport examined via Electrochemical Quartz Crystal Microbalance (EQCM).

$$R-Fc \rightarrow R-Fc^+ + e^-$$
$$R-Fc^+ + X^- \rightarrow R-Fc^+X^-$$

Typical CV profile (0.1 M $HClO_4$) of Ferrocene based electroactive alkanethiol monolayer film.

$S(CH_2)_{10}CO_2$ Fc = R-Fc

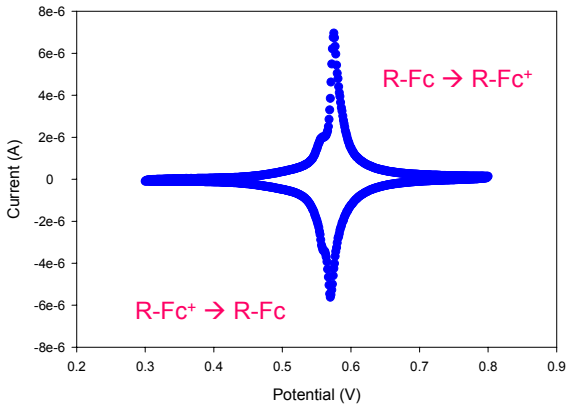

Cyclic Voltammetry study of ferrocene based electroactive thiols of varying alkane chain length.

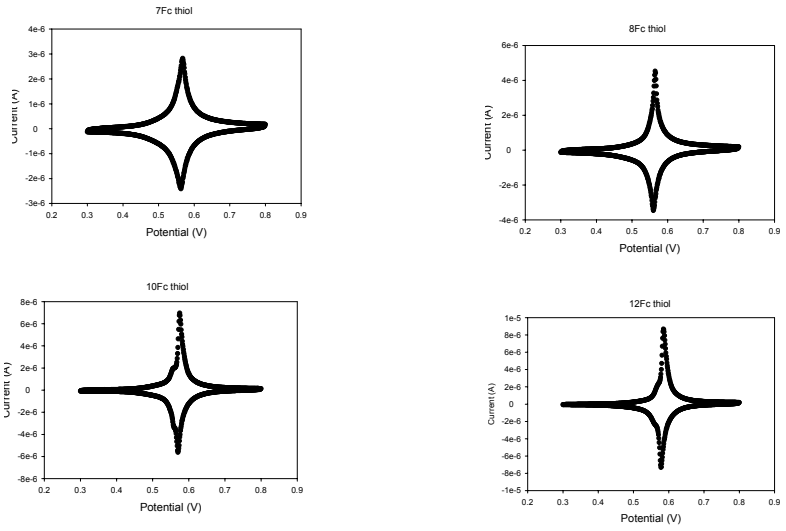

CV parameters for ferrocene containing electroactive thiols (C_n-Fc-SAM).

Alkane Chain Length	E_{PA} (mV)	E_{PC} (mV)	E^0 (mV)	ΔE (mV)	FWHM (mV)
7	568	562	565	6	35.9
8	568	560	564	8	17.7
10	575	570	573	5	15.0
12	586	578	582	8	18.0

n	$10^{10}\Gamma$/mol cm^{-2}
6	0.6
8	3.3
10	5.5
12	6.1

EQCM study of redox switching in ferrocene based SAM films.

10 Fc thiol. CV + EQCM

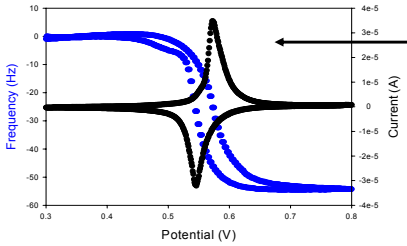

Sauerbrey Equation

$\triangle f = [-2f_0^2 / A(\mu\rho)^{1/2}] \triangle m$

For:

$\triangle f = 18.5Hz$

$\Rightarrow \triangle m = 2.59 \times 10^{-8}$ g

This is approximately equivalent to one perchlorate ion per redox site being incorporated onto the SAM surface

11Fc thiol. CV + EQCM

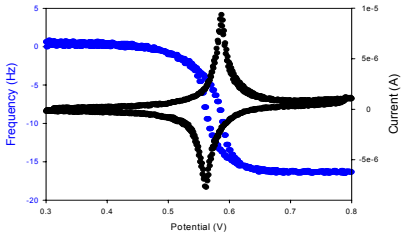

12 Fc thiol. CV + EQCM

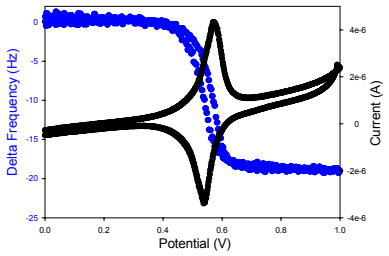

EQCM study of redox behaviour of ferrocene based electroactive thiols

Alkane Chain Length ($S(CH_2)_nCO_2Fc$)	Frequency Change (Hz)	Mass Change (g)
7	-19.6	2.70×10^{-8}
8	-18.2	2.55×10^{-8}
12	-18.5	2.59×10^{-8}

Laviron Model : LPS Voltammetry

- Assume oxidative surface redox reaction.
- Neglect interaction effects between surface immobilized groups.
- Develop normalised LPSV response of $\Psi = \Psi(\xi)$.

$$\Psi = \frac{i}{F^2 A \Gamma_\Sigma \upsilon / RT}$$

$$\xi = \frac{F}{RT}\left(E - E^0\right)$$

$$\Psi_{\mathrm{ERev}} = \frac{\exp[-\xi]}{(1+\exp[-\xi])^2} = \frac{\eta^{-1}}{(1+\eta^{-1})^2}$$

$$\Psi_{\mathrm{EIrrev}} = m\eta^\beta \exp\left[-\frac{m}{\beta}\eta^\beta\right]$$

$$\eta = \exp[\xi]$$

$$m = \frac{k^0}{\sigma} = \frac{k^0}{F\upsilon/RT}$$

E. Laviron J. Electroanal. Chem. 101 (1979) 19-28.

Theoretical LPS voltammograms: Surface redox reaction.

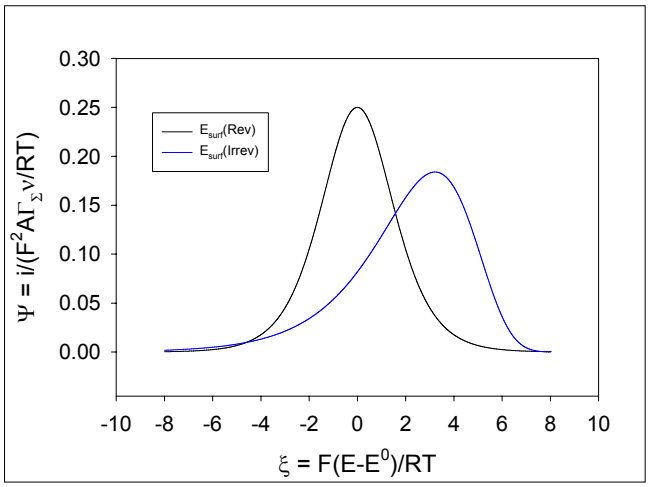

Potential Step Chronoamperometry: Quantifying Surface ET Dynamics

- Potential Step Chronoamperometry can be used to probe the dynamics of a fast surface electron transfer reaction within a monolayer film.
- Apply large amplitude potential step and monitor resulting current variation (arising from surface ET event) as a function of time.
- Ideally **first order kinetics** exhibited by surface ET process.

$$i(t) = k_{ET}\Delta Q \exp\left[-k_{ET}t\right]$$

Charge passed during transient

$$\Delta Q = nFA\Gamma_{\Sigma}$$

ET rate constant depends on potential

$$k_{ET} = k_{ET}^{0} \exp\left[\frac{\beta F\left(E - E_{A,B}^{0}\right)}{RT}\right]$$

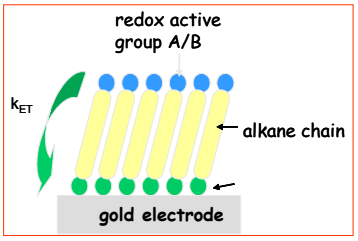

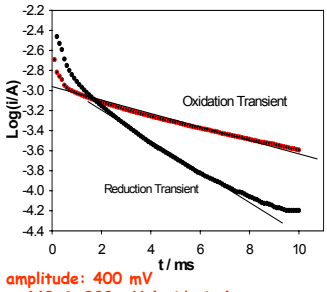

PS amplitude: 400 mV
From 440 → 880 mV (oxidation)
And 880 → 440 mV (reduction)
10 ms pulse width. C_{12}-Fc-thiol

$$k_{ET}(\text{oxidation}) = 24.1 \pm 1.5\ s^{-1}$$
$$k_{ET}(\text{reduction}) = 67.3 \pm 5.2\ s^{-1}$$

PS chronoamperometry: Fc labelled C_{12}- alkanethiol SAM film.

- PS chronoamperometric transients recorded in 1st order semi-logarithmic format for the C_{12} Fc-alkanethiol monolayer.
- Transient current response corresponds to electron tunneling through hydrocarbon chain brought about by the potential step induced surface bound ferrocene/ferricinium redox transition.
- Current Decay kinetics more rapid in the presence (black curve) of an external magnetic field of magnitude 0.5 T than in the absence (red curve) of the field .
- Potential step 300 - 850 mV (oxidation) and 850-300 mV (rediction). Timescale 10 ms. Supporting electrolyte: 0.1M HClO4.